

Generalized Finite-time Optimal Control Framework in Stochastic Thermodynamics

Atul Tanaji Mohite  ^{1,*} and Heiko Rieger  ¹

¹*Department of Theoretical Physics and Center for Biophysics, Saarland University, Saarbrücken, Germany*

(Dated: November 4, 2025)

Optimal processes in stochastic thermodynamics are a frontier for understanding the control and design of non-equilibrium systems, with broad practical applications in biology, chemistry, and nanoscale/mesoscale systems. Optimal mass transport theory and thermodynamic geometry have emerged as optimal control methodology, but they are based on slow-driving and close to equilibrium assumptions. An optimal control framework in stochastic thermodynamics for finite time driving is still elusive. Therefore, we solve in this paper an optimal control problem for changing the control parameters of a discrete-state far-from-equilibrium process from an initial to a final value in finite-time. Optimal driving protocols are derived that minimize the total finite-time dissipation cost for the driving process. Our framework reveals that discontinuous endpoint jumps are a generic, model-independent physical mechanism that minimizes the optimal driving entropy production, whose importance is further amplified for far-from-equilibrium systems. The thermodynamic and dynamic physical interpretation and understanding of discontinuous endpoint jumps is formulated. An exact mapping between the finite-time to slow driving optimal control formulation is elucidated, developing the state-of-the-art of optimal mass transport theory and thermodynamic geometry, which has been the current paradigm for studying optimal processes in stochastic thermodynamics that relies on slow driving assumptions. Our framework opens up a plethora of applications to the thermodynamically efficient control of a far-from-equilibrium system in finite-time, which opens up a way to their efficient design principles.

1. INTRODUCTION

The framework of Stochastic Thermodynamics (ST) has developed the thermodynamic understanding of mesoscopic systems [1–5]. In ST, entropy production rate (EPR) quantifies the thermodynamic dissipation cost and constrains the dynamics of non-equilibrium systems. For example, the fluctuation relation (FR) and the thermodynamic kinetic uncertainty relation (TKUR) have revealed fundamental thermodynamic laws, valid beyond the second law of thermodynamics [1, 6]. Recently, a new paradigm of optimal control problems has emerged in ST. Here, the optimal control problem is loosely defined as changing an initial state (control parameter) to a final state (control parameter) in a finite time, to compute the optimal driving protocols (change of state/control parameters) that minimize the thermodynamic dissipation. Three classes of methodologies have emerged to study optimal control.

First, optimal processes that minimize finite-time dissipation have been investigated for a stochastic particle in a harmonic trap [7]. Surprisingly, the finite-time optimal protocols were found to exhibit discontinuities at the initial and final times, namely the ‘*kinks*’. Recently, this mechanism has been understood as a mathematical artefact of the imposed boundary condition [8]. However, these works fail to capture the physical and thermodynamic origin of the ‘*kinks*’ [7, 8]. The universality of ‘*kinks*’ have been observed in some computationally solvable models [9–12]. Despite a few model-specific studies, analytically computable solutions for other models are lacking, which has created a void in the theoretical physical understanding/framework to attribute this phenomenon.

Second, thermodynamic length defines the distance in the control parameter space of a model and connects it to the

thermodynamic dissipation cost [13–16]. This Riemannian geometric structure in the control parameter space has been exploited to compute optimal driving protocols and formulate the framework of thermodynamic geometry, which is valid in the slow-driving limit. Within this framework, a geodesic is a minimum-distance path between the initial and final control parameters and is equivalently the optimal driving protocol [16, 17]. Thermodynamic geometry has advantages because of its practical applicability. In particular, metric tensors are numerically/experimentally computed for sophisticated models and systems [16–29]. Therefore, because of its practical applicability, thermodynamic geometry has been rigorously studied in comparison to the first methodology. However, thermodynamic geometry has two major drawbacks. First, it relies on the slow-driving approximation, which makes it suboptimal for finite-time optimal driving processes, where the driving time is small and the slow-driving assumption is inherently violated. See Ref.[30] for the experimentally verified violation. Second, it lacks the ‘*kinks*’ in optimal driving protocols, rendering it inconsistent with exact analytical solutions in Ref. [7–12].

Recently, a third optimal control methodology has emerged in ST, which uses a mathematical framework: the optimal mass transport theory (OMTT) [31–34]. The insights from OMTT have been incorporated into ST [35–46]. The mapping between ST and OMTT relies on the equivalence between EPR in ST and the Wasserstein distance in OMTT (an information-theoretical distance measure between probability distributions). The optimal transport map corresponds to optimally changing an initial probability distribution to a final probability distribution; equivalently, the optimal driving protocol is obtained here. Hence, the optimal control in OMTT assumes ‘full’ control of the probability distribution defined in the state-space; in comparison, thermodynamic geometry assumes a parametric control defined in the control parameter space. Due to its inherent formulation as an

* atul.mohite@uni-saarland.de

optimization problem, OMTT has a broad range of statistical machine learning applications and advantages [47], to name a few, computer vision, linguistic, signal, and image representation.

Despite its multitude of successful applications, OMTT has three major drawbacks. First, despite the numerical applicability of OMTT, exact analytical solutions are not available except for Gaussian systems, a statistical approximation that does not necessarily hold for finite-size systems in ST prone to non-Gaussian fluctuations [48, 49]. Second, the quadratic dependence of EP on driving, it is an assumption that holds for systems close-to-equilibrium (cEQ) [5, 48–50], and leads to a massive underestimation of EP for far-from-equilibrium (fEQ) systems [48, 49]. Third, when the driving time to reach the initial to final state is finite, driving time is a resource to be optimized over, OMTT does not take this constraint into account, which results in its suboptimal performance for a finite-time optimal process, since OMTT is built upon the slow driving assumption. Therefore, the results obtained using OMTT are inconsistent with the model-specific exact analytical results from Ref.[7, 9], the ‘*kinks*’ are absent even for the most simple models; see Ref.[51] for a comparison.

The total EP has three linearly independent contributions, namely driving work, excess EP, and housekeeping EP [5, 49]. They physically correspond to dissipation due to total free energy, relaxation towards the Boltzmann distribution, and sustaining nonconservative forces, respectively. However, in the work discussed so far, the focus of optimization has been on driving work or excess EPR. The optimization of the housekeeping EPR has been completely lacking, which quantifies the thermodynamic cost of sustaining non-equilibrium currents. In addition, the focus has been on continuous-state systems, instead of discrete-state systems. Where, due to the non-quadratic dependence of the EPR on driving affinity in discrete-state systems, cEQ optimal control methods are physically less relevant, as they assume a quadratic dependence of the EPR on driving affinity and neglect housekeeping EPR [48, 49]. Despite attempts to understand the finite-time optimal processes consistent in ST, inconsistencies and discrepancies persist, and a coherent unified framework and understanding of the finite-time optimal control in ST is lacking.

Due to their better computational aspects, variational formulations of physical processes have been utilized to study the dynamics of non-equilibrium systems, for instance, phase transitions, first-passage times, and metastability in stochastic systems [52–59]. Variational formulations have broad applicability for efficient numerical optimization problems in machine learning [60–62], and have recently been explored in ST [63–68]. Recently, an exact variational formulation for fEQ discrete-state processes has been formulated, namely, the ‘Minimum action principle’ (MinAP) [48, 49], an exact canonical ensemble analog of non-equilibrium discrete-state systems, that connects the transition probability measure to thermodynamic and dynamic physical quantities, namely entropy production and thermodynamic length of transition currents/traffics. The application of MinAP unifies FR and the non-quadratic formulation of TKUR within a single

framework [48, 49].

Here, based on MinAP [48, 49], we formulate the generalized finite-time optimal control (GFTOC) framework valid for any discrete-state fEQ system, by exploiting the Riemannian geometric structure in the control parameter space. We compute the optimal finite-time driving protocols that minimize the total driving EP, which exhibit the ‘*kinks*’. GFTOC unifies the optimal control of slowly driven and finite-time processes, as we prove an exact mapping between them. Importantly, since MinAP assigns a thermodynamic cost for any transition path realization, a thermodynamic cost for sustaining the ‘*kinks*’ is quantified (a boundary term in driving time), namely ‘thermodynamic shock’. Thereby, the ‘*kinks*’ reduce the thermodynamic cost of driving (a bulk term in driving time), since the ‘*kinks*’ reduce the distance to be travelled in the control parameter space. The thermodynamic interplay between the boundary and the bulk terms of driving EP gives rise to the formation of the ‘*kinks*’ as a dynamic consequence. The dual manifestation of the bulk-boundary term of EP driving has a physical interpretation analogous to the work-heat, but formulated here for the finite-time optimal process in ST. We show that the dynamic counterpart of this thermodynamic phenomena is dictated by the restoration of the ‘finite-time speed limit’: an inherent physical timescale associated with the optimal driving process.

We exhibit the applicability of GFTOC using different examples. We address consistency issues associated with the aforementioned different model-specific formulations of optimal control methodologies, and a unified and universal theoretical framework of optimal control in stochastic thermodynamics is unveiled. Our framework formulates a three-fold realization of MinAP in ST as; non-quadratic TKUR, FR, and GFTOC, which correspond to thermodynamic inference, partial control, and full control descriptions, respectively [48]. A ‘full control’ description using GFTOC propels the thermodynamically efficient design and control (in a finite-driving time) of finite-size stochastic systems where stochastic thermodynamics has been experimentally proven theoretical framework. The stochastic thermodynamic insight of the ‘*kinks*’ formulated by GFTOC develops state-of-the-art of OMTT and Thermodynamic geometry, both of which have exhibited a multitude of practical applications but are based on the slow driving assumption. It is an interesting avenue to explore the practical and interdisciplinary implications of GFTOC in OMTT and Thermodynamic geometry.

SETUP

Thermodynamically consistent discrete-state systems and graphs. — We model thermodynamically consistent discrete-state systems using a Markov jump process (MJP) or a chemical reaction network (CRN) represented by a graph [69]. ρ_i denotes the probability/density of the state, which is a node of the graph. The set of all discrete states is denoted by $\{i\}$. γ^{\Rightarrow} denotes the set of forward and backward transitions between states ρ_i and ρ_j , with J_Y and A_Y denoting the current and affinity for the transition γ^{\Rightarrow} between states. $\{\gamma^{\Rightarrow}\}$ de-

notes the set of all bidirectional transitions of the graph. The transitions satisfy the Local detailed balance condition (LDB), $A_\gamma = \log(j_\gamma/j_{-\gamma}) = F_\gamma - \Delta_\gamma E + \Delta_\gamma S_i^{state}$, where j_γ and $j_{-\gamma}$ are the forward and backward transition currents satisfying $J_\gamma = j_\gamma - j_{-\gamma}$. The transition affinity A_γ is decomposed into an external non-conservative driving F_γ , a change in the equilibrium energy functional $\Delta_\gamma E$, and a change in the state entropy $S_i^{state} = -\log(\rho_i)$ [2]. The energy functional $E(\{\lambda_E\})$ is fully controlled using the set of control parameters $\{\lambda_E\}$.

The symmetric component of the transition currents is called the traffic and is defined as $T_\gamma = j_\gamma + j_{-\gamma}$. The transition mobility is defined as $D_\gamma = \sqrt{j_\gamma j_{-\gamma}}$, and it is time-symmetric, quantifying the amplitude of the transition currents. This allows us to define hyperbolic relations between different basis $\{A_\gamma, D_\gamma\} \rightarrow \{J_\gamma, T_\gamma\} : J_\gamma = 2D_\gamma \sinh(A_\gamma/2)$ and $T_\gamma = 2D_\gamma \cosh(A_\gamma/2)$. Basis $\{J_\gamma, T_\gamma\}$ and $\{A_\gamma, D_\gamma\}$ formulate the thermodynamic inference and full control descriptions, respectively. This nomenclature is attributed to the affinities $\{A_\gamma\}$ and the mobilities $\{D_\gamma\}$ being the controllable physical parameters, which physically correspond to controlling the current asymmetry and amplitude, respectively [5].

We introduce a shorthand notation for the state-space column vector $\vec{\rho} = (\dots, \rho_i, \dots)^T$ and the current-space vector $\vec{J} = (\dots, J_\gamma, \dots)^T$. Therefore, the continuity equation for the transport of probabilities/densities is,

$$\partial_t \vec{\rho} = \mathbb{S} \vec{J}. \quad (1)$$

The stoichiometry matrix \mathbb{S} encodes the topology of the transition space $\{\gamma^\rightleftharpoons\}$. It contracts the transition currents $\{J_\gamma\}$ to the state-space $\{\rho_i\}$. The entries \mathbb{S}_{ij} of \mathbb{S} are 1 or -1 if state ρ_i is part of a transition $\gamma^\rightleftharpoons$, and the sign convention is decided by the direction of transition currents; otherwise, $\mathbb{S}_{ij} = 0$.

Thermodynamic dissipation of graphs. — The mean EPR for the graph satisfies the bilinear form $\langle \dot{\Sigma} \rangle = \sum_{\{\gamma^\rightleftharpoons\}} J_\gamma A_\gamma$, which physically corresponds to the thermodynamic dissipation being equal to the driving force (affinity) multiplied by the current generated by it. Furthermore, the mean EPR $\langle \dot{\Sigma} \rangle$ for the graph is decomposed into three linearly independent orthogonal contributions [49],

$$\begin{aligned} -\dot{\psi}_E &= -\dot{\lambda}_E \partial_{\lambda_E} \psi_E, \\ \langle \dot{\Sigma}_E^{ex} \rangle &= \sum_{\{i\}} d_t \rho_i \log \left(\frac{\rho_i}{\rho_i^E} \right) = -d_t D_E^{KL}, \\ \langle \dot{\Sigma}^{hk} \rangle &= \sum_{\{\gamma^\rightleftharpoons\}} T_\gamma^\perp F_\gamma \sinh \left(\frac{F_\gamma}{2} \right). \end{aligned} \quad (2)$$

These are quasi-static work, excess, and housekeeping EPR, respectively. They physically correspond to the driving of the functional energy E through a set of external control parameters $\{\lambda_E\}$, the relaxation toward the Boltzmann distribution dictated by E , and the sustained dissipative transition currents due to non-conservative forces $\{F_\gamma\}$, respectively. $-\dot{\psi}_E$ and $\dot{\Sigma}_E^{ex}$ are the boundary terms in the control parameter space and the state space, respectively [5, 49]. $-\dot{\psi}_E$ is integrated over time to obtain the free-energy difference between

the initial and final control parameters, $\psi_E(\lambda_E^{inl}) - \psi_E(\lambda_E^{fnl})$. Similarly, the KL divergence (D_E^{KL}) quantifies the statistical distance of the instantaneous state-space distribution from the equilibrium Boltzmann distribution, $\rho_i^E = e^{-E_i + \psi_E}$. Thus, a time-integrated excess EPR yields an excess EP, which is the difference between the initial and final state-space distributions and is defined with respect to the initial and final control parameters, $\Sigma_E^{ex} = -\Delta_0^{KL}$. It is simplified to $\Sigma_E^{ex} = D_E^{KL}(\lambda_E^{inl}, t = 0) - D_E^{KL}(\lambda_E^{fnl}, t = \tau)$, with $D_E^{KL}(\lambda_E^{inl}, t = 0) = \sum_{\{\rho_i\}} \rho_i^{inl} \log \left(\rho_i^{inl} / \rho_i^E(\lambda_E^{inl}) \right)$ and $D_E^{KL}(\lambda_E^{fnl}, t = \tau) = \sum_{\{\rho_i\}} \rho_i^{fnl} \log \left(\rho_i^{fnl} / \rho_i^E(\lambda_E^{fnl}) \right)$. The mean housekeeping EPR $\langle \dot{\Sigma}^{hk} \rangle$ is a non-quadratic function of the non-conservative driving force F_γ multiplied by the equilibrium traffic T_γ^\perp (the direction orthogonal to the external driving). T_γ^\perp quantifies the scaled equilibrium diffusion constant defined for $\gamma^\rightleftharpoons$ due to the equilibrium thermodynamic activity of the states ρ_i and ρ_j . For example, for MJP/ideal CRN, $T_\gamma^\perp = \rho_i + \rho_j$, and for interacting CRN, $T_\gamma^\perp = \rho_i e^{\mu_i^{int}} + \rho_j e^{\mu_j^{int}}$, where μ_i^{int} is the chemical potential of ρ_i attributed to non-ideal interactions of ρ_i [5, 50].

Minimum action principle. — The transition probability measure for discrete-state processes is equal to the exponential of an action $\mathcal{S}[\{A_\gamma, D_\gamma\}]$ [48–50],

$$\mathcal{P}[\{A_\gamma, D_\gamma\}] = e^{-\mathcal{S}[\{A_\gamma, D_\gamma\}]} \quad (3)$$

where the action $\mathcal{S}[\{A_\gamma, D_\gamma\}] = \int_0^\tau dt \mathcal{L}^*[\{A_\gamma, D_\gamma\}]$ is a time-integral of the effective transition Lagrangian, which equivalently quantifies the effective mean EPR,

$$\langle \dot{\Sigma} \rangle = \mathcal{L}^*[\{A_\gamma, D_\gamma\}] = \sum_{\{\gamma^\rightleftharpoons\}} 2D_\gamma A_\gamma \sinh \left(\frac{A_\gamma}{2} \right), \quad (4)$$

represented here in the ‘full’ control description using the transition mobility D_γ and transition affinity A_γ . Equations (3) and (4) are key results of Refs. [48, 49], and formulate a variational principle for discrete-state processes. In particular, the analytical solution for the dynamics of discrete-state processes is obtained by analytically/numerically solving the variational problem for $\mathcal{L}^*[\{A_\gamma, D_\gamma\}]$, namely, the ‘Minimum action principle’ (MinAP). We will exploit the MinAP framework to formulate and solve the GFTOC problem.

2. SLOW DRIVING OPTIMAL CONTROL

We consider a GFTOC problem of slow driving of the effective Lagrangian \mathcal{L}^* in eq. (4) from the initial A_α^i to the final control parameter A_α^f in a time τ that minimizes the EPR required for the driving process, which is implemented through external parametric control of A_α . Here, the control of transition affinity A_α is generally used to denote multiple linearly independent control parameters that can implement this. Three linearly independent cases of affinity control correspond to independently contributed EPR, namely

$-\partial_t \psi_E$, $\langle \dot{\Sigma}_E^{ex} \rangle$, and $\langle \dot{\Sigma}^{hk} \rangle$, quantified by the corresponding effective Lagrangians and relevant controllable affinities are $\{\lambda_E\}$, $\{-\log(\rho_i/\rho_i^E)\}$, and $\{F_\gamma\}$, respectively.

2.1. Geodesic structure

We consider slow driving of the Lagrangian, which physically implies that the system dynamics and statistics quickly adapt to the instantaneous control parameters. Hence, the slow driving formulation is valid under a timescale separation, precisely, only if the driving timescale is slower than the coupling timescale between the environment and the system or the relaxation timescale of the system, which quantifies how quickly the system adapt to the instantaneously imposed control parameters. Under the assumption of slow driving, we expand the Lagrangian to second-order terms in the rate of driving \dot{A}_α . The driving Lagrangian reads [13–15]:

$$\mathcal{L}_{drv}^* [A_\alpha, \dot{A}_\alpha] = \frac{1}{2} \partial_\alpha^2 \mathcal{L}^* (\dot{A}_\alpha)^2, \quad (5)$$

such that the total driving EP is $\Sigma_{drv}^{qs} = \Sigma_{drv}^* = \int_0^\tau dt \mathcal{L}_{drv}^*$. Equation (5) quantifies the driving kinetic energy, where the mass is given by the instantaneous curvature of the Lagrangian ($\partial_\alpha^2 \mathcal{L}^*$). We adopt the shorthand notation $\partial_\alpha^2 \mathcal{L}^* = \partial_{A_\alpha}^2 \mathcal{L}^* = D_\alpha [2 \cosh(A_\alpha/2) + \frac{1}{2} A_\alpha \sinh(A_\alpha/2)] = T_\alpha + \frac{1}{4} \mathcal{L}^*$.

The fEQ driven systems (with a larger A_α) exhibit a higher mass, attributed to larger fluctuations (T_α) and dissipation (\mathcal{L}^*). Physically, this signifies a higher resistance to the driving for fEQ systems, fig. 1(a). fEQ driving is slowed due to increased resistance, with a singularity in the $A_\alpha \rightarrow \infty$ limit caused by divergence of the EPR and traffic. Importantly, the local curvature $\partial_\alpha^2 \mathcal{L}^*$ generalizes the stochastic Fisher information for any \mathcal{L}^* . Choosing excess EP as the total dissipation cost shows the equivalence between mass and stochastic Fisher information for each state, discussed subsequently below. We have omitted the potential energy boundary term, namely, the instantaneous EPR, which does not depend on driving speed and time, and corresponds to the unavoidable instantaneous minimum EPR cost. This reduces the slow-driving optimization problem to a minimization problem of the driving kinetic energy (driving EPR). Its solution is the geodesic equation for A_α ,

$$\ddot{A}_\alpha + \frac{\partial_\alpha^3 \mathcal{L}^*}{2 \partial_\alpha^2 \mathcal{L}^*} \dot{A}_\alpha^2 = 0, \quad (6)$$

eq. (6) generalizes the geodesic equation for the optimal control of fEQ systems that minimizes driving EPR [17]. It equivalently implies $\dot{A}_\alpha \sqrt{\partial_\alpha^2 \mathcal{L}^*} = v_{qs}$, where v_{qs} is the quasi-static driving speed along the geodesic in the driving time τ . The minimum action solution for optimal driving is called the geodesic and is denoted by $\mathcal{G}(A_\alpha)$. It encodes the minimum distance path in the control parameter space, and its analytical form plays a crucial role. By definition, the geodesic implies $\mathcal{G}(A_\alpha) = \arg \inf_{A_\alpha} (\Sigma_{drv}^{qs})$, and the corresponding minimum EP is $\Sigma_{qs}^* = \inf_{A_\alpha} (\Sigma_{drv}^{qs})$, under the initial and final

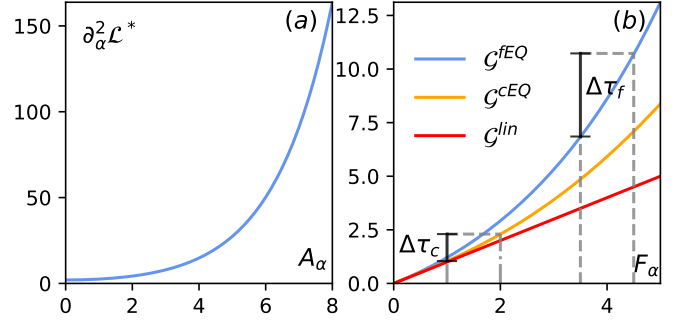


FIG. 1. (a) The curvature of the Lagrangian $\partial_\alpha^2 \mathcal{L}^*$ (mass) increases exponentially for the higher value of driving affinity A_α . (b) $\mathcal{G}(F_\alpha) : F_\alpha \rightarrow t$. Comparison between $\mathcal{G}^{fEQ}(F_\alpha)$, $\mathcal{G}^{cEQ}(F_\alpha)$ and $\mathcal{G}^{lin}(F_\alpha)$ given by eq. (9). For the fixed quasi-static driving speed v_{qs} , $F_\alpha^f - F_\alpha^i = 1$ is considered for the cEQ $F_\alpha^i = 1$ and fEQ $F_\alpha^i = 3.5$ and the corresponding $\Delta\tau_c$ and $\Delta\tau_f$ are plotted; it is a combined pictorial visualization of eqs. (9) and (13). Due to eq. (13), the speed limit for the quasi-static slow-driving increases for fEQ systems, an effect attributed to the higher mass required for the driving of fEQ systems.

boundary conditions A_α^i and A_α^f . Thus, $\dot{A}_\alpha \propto 1/\sqrt{\partial_\alpha^2 \mathcal{L}^*}$ implies that A_α has to be driven slower the further the system is from equilibrium. Physically, this means that for the validity of the optimal driving, each infinitesimally small driving timestep Δt contributes equally to Σ_{drv}^{qs} .

Computing the geodesic gives the mapping between driving speed, time, and control parameter, $A_\alpha(t) = \mathcal{G}^{-1}(v_{qs}t)$. Here, $\mathcal{G}(A_\alpha) : A_\alpha \rightarrow t$ is a function mapping the instantaneous control parameter to time. Its inverse function is $\mathcal{G}^{-1}(v_{qs}t) : t \rightarrow A_\alpha$. Thus, in geodesic space, the driving protocol satisfies the linear solution $\mathcal{G}(A_\alpha) = c_0 + v_{qs}t$, with c_0 and v_{qs} being unknowns to be determined. To this end, slow driving inherently imposes the boundary conditions at the initial and final times. Hence, $\mathcal{G}(A_\alpha^i) = c_0$ and $\mathcal{G}(A_\alpha^f) = v_{qs}\tau + c_0$, which imply $c_0 = \mathcal{G}(A_\alpha^i)$ and $v_{qs} = [\mathcal{G}(A_\alpha^f) - \mathcal{G}(A_\alpha^i)]/\tau$. This reduces the optimal driving protocol to a linear interpolation in geodesic space between the initial and final control parameters:

$$\mathcal{G}(A_\alpha) = \left(1 - \frac{t}{\tau}\right) \mathcal{G}(A_\alpha^i) + \frac{t}{\tau} \mathcal{G}(A_\alpha^f) \quad (7)$$

Hence, $v_{qs} = \partial_t \mathcal{G}(A_\alpha) = \frac{1}{\tau} [\mathcal{G}(A_\alpha^f) - \mathcal{G}(A_\alpha^i)]$. It simplifies $\Sigma_{qs}^* = \inf_{A_\alpha} (\Sigma_{drv}^{qs}) = \inf_{A_\alpha} \int_0^\tau \mathcal{L}_{drv}^* dt = \frac{1}{2} \tau (v_{qs})^2 = \frac{1}{2} \tau (\partial_t \mathcal{G}(A_\alpha))^2$. Thus, the minimum slow-driving EP cost reads,

$$\Sigma_{qs}^* = \frac{1}{2\tau} \left(\mathcal{G}(A_\alpha^f) - \mathcal{G}(A_\alpha^i) \right)^2. \quad (8)$$

This simplification allows us to visualize the physical meaning of geodesic space. In particular, the optimal control problem for A_α with a varying instantaneous local mass is converted into one with a unit mass using the geodesic map $\mathcal{G}(A_\alpha)$. Similarly, time is scaled in units of the driving time

τ . This mapping converts the non-quadratic optimal control problem in A_α space to a quadratic optimal control problem in $\mathcal{G}(A_\alpha)$ with a scaled unit mass and a scaled unit time. This is a fundamental non-equilibrium scale-invariance relation for the optimal quasi-static driving of fEQ systems, and it delineates the underlying fundamental universality of all quasi-statically driven systems.

2.2. Exact analytical expressions for geodesics

In this section, we compute the exact analytical expressions for the geodesic for the control of transition affinity A_α for three different cases. We fix the amplitude of mass to 1 in the $A_\alpha \rightarrow 0$ limit. The first case is the linear geodesic \mathcal{G}^{lin} , which is computed using the equilibrium approximation of mass $\partial_{A_\alpha}^2 \mathcal{L}^* = 1$. The second case is the close-to-equilibrium geodesic \mathcal{G}^{cEQ} , which is computed using the close-to-equilibrium approximation. Up to $O(A_\alpha^2)$ terms of $\partial_{A_\alpha}^2 \mathcal{L}^*$, this implies $\partial_{A_\alpha}^2 \mathcal{L}^* = 1 + A_\alpha^2/4$. The third case is the fEQ geodesic \mathcal{G}^{fEQ} , which is computed using the fEQ approximation of $\partial_{A_\alpha}^2 \mathcal{L}^*$ using $\cosh(a) = \sinh(a) = \frac{1}{2}e^a$, implying $\partial_{A_\alpha}^2 \mathcal{L}^* = \frac{1}{4}(A_\alpha + 4)e^{\frac{1}{2}A_\alpha}$.

The geodesic is obtained by solving the ODE $\dot{A}_\alpha \sqrt{\partial_{A_\alpha}^2 \mathcal{L}^*} = v_{qs}$. In addition, we have imposed the constraint $\mathcal{G}(0) = 0$, which corresponds to fixing the integration constant. This allows us to compare different geodesics from the same reference point. The exact closed-form analytical expressions for the linear geodesics \mathcal{G}^{lin} , close-to-equilibrium geodesics $\mathcal{G}^{cEQ}(A_\alpha)$ and fEQ geodesics $\mathcal{G}^{fEQ}(A_\alpha)$ are:

$$\begin{aligned} \mathcal{G}^{lin}(A_\alpha) &= A_\alpha, \\ \mathcal{G}^{cEQ}(A_\alpha) &= \frac{1}{4}A_\alpha \sqrt{4 + A_\alpha^2} + \sinh^{-1}\left(\frac{A_\alpha}{2}\right), \\ \mathcal{G}^{fEQ}(A_\alpha) &= 2\sqrt{(4 + A_\alpha) e^{\frac{1}{2}A_\alpha}} - \frac{2\sqrt{\pi}}{e} \text{Erf}I\left[\frac{1}{2}\sqrt{4 + A_\alpha}\right] \\ &\quad - 4 + \frac{2\sqrt{\pi}}{e} \text{Erf}I[1], \end{aligned} \quad (9)$$

respectively. Here, $\text{Erf}I[x]$ is the imaginary error function. The analytical form of $\mathcal{G}(A_\alpha)$ plays a key role. \mathcal{G}^{fEQ} , \mathcal{G}^{cEQ} , and \mathcal{G}^{lin} are plotted in fig. 1(b). The geodesics satisfy the hierarchy of inequalities,

$$\mathcal{G}^{fEQ}(A_\alpha) \geq \mathcal{G}^{cEQ}(A_\alpha) \geq \mathcal{G}^{lin}(A_\alpha). \quad (10)$$

In $A_\alpha \rightarrow 0$ limit, $\mathcal{G}^{lin}(A_\alpha)$, $\mathcal{G}^{cEQ}(A_\alpha)$, and $\mathcal{G}^{fEQ}(A_\alpha)$ converge. However, the further the system is from equilibrium, the greater the quantitative difference is observed. The physical implication is a tighter bound on the exact optimal driving EP in eq. (8), and the deviation of the optimal driving protocol eq. (7) from a trivial linear interpolation between the initial and final control parameters. This highlights the importance of the exact fEQ geodesics.

2.3. Far-from-equilibrium generalizations of Optimal mass transport theory

The geodesic hierarchy eq. (10) implies the hierarchy $(\mathcal{G}^{fEQ}(A_\alpha^f) - \mathcal{G}^{fEQ}(A_\alpha^i))^2 \geq (\mathcal{G}^{cEQ}(A_\alpha^f) - \mathcal{G}^{cEQ}(A_\alpha^i))^2 \geq (A_\alpha^f - A_\alpha^i)^2$. Using eq. (8), for a fixed τ , a hierarchy on the driving EP reads,

$$\Sigma_{qs}^{*fEQ} \geq \Sigma_{qs}^{*cEQ} \geq \Sigma_{qs}^{*lin}. \quad (11)$$

$\mathcal{G}^{lin}(A_\alpha)$ is the special case that has been utilized in the OMTT [31, 32], and applied to ST to obtain Σ_{qs}^{*lin} as the driving cost of EP, which is quadratic function of the change in the driving affinity [35, 43]. However, the computation of \mathcal{G} takes into account the non-quadratic nature of the dissipation function \mathcal{L}^* , which results in the tightest and exact bound using eq. (11). Moreover, the right-hand side of eq. (8) is equal to the square of the \mathcal{W}_2 Wasserstein distance defined in the geodesic space of control parameters. Thus, eq. (8) leads to equality between the driving EP in stochastic thermodynamics and the Wasserstein distance in OMTT,

$$\Sigma_{qs}^* = \frac{\mathcal{W}_2^2}{2\tau} \quad (12)$$

Therefore, our optimal control formulation goes beyond the existing quadratic counterparts formulated using the OMTT [35, 43, 44, 51]. Importantly, our slow-driving formulation also generalizes the connection between ‘thermodynamic geometry’ and ‘OMTT’ beyond known quadratic formulations. This extends the applicability of ‘OMTT’ to non-Euclidean (Riemannian) control parameter manifolds.

2.4. Speed limit for slow driving

The validity of slow driving is a key assumption in the optimal control framework developed so far. Equation (8) reveals an inherent timescale associated with the driving process. Inverting eq. (8), we define the quasi-static driving timescale:

$$\tau_{qs}^* = \frac{(\mathcal{G}(A_\alpha^f) - \mathcal{G}(A_\alpha^i))^2}{2\Sigma_{qs}^*}. \quad (13)$$

τ_{qs}^* is a quantitative measure of the time required for the given initial and final control parameters (A_α^i and A_α^f) and the driving EP Σ_{qs}^* . It quantifies the timescale for the violation of the slow-driving assumption. Physically, it is equal to the square of the distance travelled along the geodesic in the control parameter space divided by the quasi-static EP supplied for the driving process. The quasi-static driving time reveals the fundamental tradeoff between the driving time and dissipation for the optimally driven process, and defines the speed limit for the slow-driving process. Importantly, the slow-driving assumption is violated for any τ and does not necessarily require $\tau \leq \tau_{qs}^*$. For the fixed value $\Delta A_\alpha = A_\alpha^f - A_\alpha^i$ and

a fixed available budget for driving EP Σ_{qs}^* , eq. (10) implies $\tau_{qs}^{*fEQ} > \tau_{qs}^{*cEQ} > \tau_{qs}^{*lin}$, see fig. 1(b). Hence, fEQ systems require a larger quasi-static driving time, attributed to critical slowing due to higher traffic and EPR. This implies that fEQ systems are more prone to breaking the assumption of slow-driving, with prominent consequences discussed subsequently in section 3.

3. FINITE-TIME OPTIMAL CONTROL

The finite-time optimal protocol exhibits discontinuous jumps at the endpoints of the protocol, namely, *kinks* [7, 8, 35, 38]. In contrast, the slow-driving approach misses such jumps [17]. The optimal slow-driving control framework developed in section 2 relies on the key assumption of a timescale separation between the driving time τ and the largest inherent relaxation timescale of the system. This implies that the system relaxes instantaneously to the control parameter dictated by the environment, justifying the quasi-static slow-driving assumption. However, finite-time optimal processes could operate on shorter timescales such that $\tau < \tau_{qs}^*$, violating the slow-driving assumption. Moreover, the slow-driving assumption is also violated for $\tau \geq \tau_{qs}^*$, except in the $\tau \rightarrow \infty$ limit. To this purpose, in this section we develop the finite-time optimal control framework, relying on the MinAP combined with the slow-driving optimal control and the geodesic structure.

3.1. Finite-time geodesic structure

In a finite-time driving process, the system realizes that it cannot quasi-statically follow the geodesic. The GFTOC formulation therefore implies that the constraint of the boundary condition on the geodesic has to be relaxed, and needs to be treated as an optimization parameter. We consider $\mathcal{G}(A_\alpha^{i*})$ and $\mathcal{G}(A_\alpha^{f*})$ as the optimal control parameter values in the geodesic space at $t = 0^+ > 0$ and $t = \tau^- < \tau$, respectively. Here, 0^+ and τ^- are infinitesimal times after the initial and before the final time, respectively. Hence, the protocol jumps in the geodesic space at the initial and final times are $\Delta_{0+}\mathcal{G}_\tau(A_\alpha) = \mathcal{G}(A_\alpha^{i*}) - \mathcal{G}(A_\alpha^i)$ and $\Delta_{\tau^-}\mathcal{G}_\tau(A_\alpha) = \mathcal{G}(A_\alpha^f) - \mathcal{G}(A_\alpha^{f*})$, where we have chosen the convention $\mathcal{G}(A_\alpha^i) \leq \mathcal{G}(A_\alpha^{i*}) < \mathcal{G}(A_\alpha^{f*}) \leq \mathcal{G}(A_\alpha^f)$, which need not be imposed as the optimal solution ensures this hierarchical inequality. The slow-driving is followed along the geodesic from $\mathcal{G}(A_\alpha^{i*})$ to $\mathcal{G}(A_\alpha^{f*})$ from time 0^+ to τ^- . Within the MinAP [48, 49], the thermodynamic EP cost associated with *kinks* is the boundary term $\Sigma_{bnd} = \int \mathcal{L}_{bnd}^* [A_\alpha] = \frac{1}{2} (\Delta_{\tau^-}\mathcal{G}_\tau(A_\alpha))^2 + \frac{1}{2} (\Delta_{0+}\mathcal{G}_\tau(A_\alpha))^2$, which penalizes the formation of *kinks*. The bulk EP to drive along the geodesic from $\mathcal{G}(A_\alpha^{i*})$ to $\mathcal{G}(A_\alpha^{f*})$ is modified to $\Sigma_{bulk} = \int_{0^+}^{\tau^-} \mathcal{L}_{bulk}^* dt = \frac{1}{2\tau} (\mathcal{G}(A_\alpha^{f*}) - \mathcal{G}(A_\alpha^{i*}))^2$. Since $|\mathcal{G}(A_\alpha^{i*}) - \mathcal{G}(A_\alpha^{f*})| < |\mathcal{G}(A_\alpha^i) - \mathcal{G}(A_\alpha^f)|$, it follows that $\Sigma_{bulk} < \Sigma_{qs}^*$. Hence, the increase in Σ_{bnd} due to *kinks* is com-

pensated by a decrease in Σ_{bulk} , and their interplay plays a key role in optimal finite-time protocols.

The total EP associated with the GFTOC problem is $\Sigma_\tau = \Sigma_{bnd} + \Sigma_{bulk}$. Within the MinAP [48, 49], the minimization of Σ_τ requires solving the variational optimal control problem with unknown free parameters $A_\alpha^{i*}, A_\alpha^{f*}$,

$$\Sigma_\tau^* = \inf_{\{A_\alpha^{i*}, A_\alpha^{f*}\}} (\Sigma_\tau). \quad (14)$$

The variation with respect to A_α^{i*} and A_α^{f*} leads to the following set of linear Euler-Lagrange equations $\frac{\delta \Sigma}{\delta \mathcal{G}(A_\alpha^{i*})} = 0, \frac{\delta \Sigma}{\delta \mathcal{G}(A_\alpha^{f*})} = 0$, whose reorganization leads to,

$$\begin{aligned} \left(1 + \frac{1}{\tau}\right) \mathcal{G}(A_\alpha^{i*}) - \frac{1}{\tau} \mathcal{G}(A_\alpha^{f*}) &= \mathcal{G}(A_\alpha^i), \\ -\frac{1}{\tau} \mathcal{G}(A_\alpha^{i*}) + \left(1 + \frac{1}{\tau}\right) \mathcal{G}(A_\alpha^{f*}) &= \mathcal{G}(A_\alpha^f). \end{aligned} \quad (15)$$

Inverting eq. (15), its solution reads:

$$\begin{aligned} \mathcal{G}(A_\alpha^{i*}) &= \frac{1 + \tau}{2 + \tau} \mathcal{G}(A_\alpha^i) + \frac{1}{2 + \tau} \mathcal{G}(A_\alpha^f), \\ \mathcal{G}(A_\alpha^{f*}) &= \frac{1}{2 + \tau} \mathcal{G}(A_\alpha^i) + \frac{1 + \tau}{2 + \tau} \mathcal{G}(A_\alpha^f). \end{aligned} \quad (16)$$

The corresponding finite-time optimal protocol reads:

$$\begin{aligned} \mathcal{G}_\tau(A_\alpha) &= \mathcal{G}(A_\alpha^i), & t = 0, \\ &= \left(1 - \frac{t}{\tau}\right) \mathcal{G}(A_\alpha^{i*}) + \frac{t}{\tau} \mathcal{G}(A_\alpha^{f*}), & t \in (0, \tau), \\ &= \mathcal{G}(A_\alpha^f), & t = \tau. \end{aligned} \quad (17)$$

Equivalently, using eq. (16), the finite-time optimal protocol for $t \in (0, \tau)$ can be expressed using the known control parameters $\mathcal{G}(A_\alpha^i)$ and $\mathcal{G}(A_\alpha^f)$ as

$$\mathcal{G}_\tau(A_\alpha) = \left(\frac{1 + \tau}{2 + \tau} - \frac{t}{2 + \tau}\right) \mathcal{G}(A_\alpha^i) + \left(\frac{1}{2 + \tau} + \frac{t}{2 + \tau}\right) \mathcal{G}(A_\alpha^f). \quad (18)$$

Equation (18) is the optimal finite-time transport map. It is equivalent to substituting $t/\tau \rightarrow t/(\tau + 2)$, $1 \rightarrow (1 + \tau)/(2 + \tau)$, and $0 \rightarrow 1/(2 + \tau)$ in eq. (7). Physically, optimal finite-time driving is equivalent to total driving time $\tau + 2$ with initial and final times $t = 1$ and $t = \tau + 1$, respectively, leading to jumps in the optimal protocol at the endpoints. This reveals the structural geometric similarities between the finite-time optimal driving and the slow-driving process.

Using eq. (18), the amplitude of *kinks* is quantified as $\Delta_{0+}\mathcal{G}_\tau(A_\alpha) = \Delta_{\tau^-}\mathcal{G}_\tau(A_\alpha) = \frac{1}{2+ \tau} (\mathcal{G}(A_\alpha^f) - \mathcal{G}(A_\alpha^i))$. Hence, *kinks* are of equal amplitude in geodesic space, which physically corresponds to equal distribution of the thermodynamic cost associated with *kinks*. Upon converting back to the control parameter space A_α using \mathcal{G}^{-1} , *kinks* have different amplitudes. The higher-mass endpoint has a smaller jump size

compared to the lower-mass endpoint. The amplitude of *kinks* scales as $1/(2 + \tau)$, vanishing in the quasistatic limit $\tau \rightarrow \infty$. For the fast-driving limit $\tau \rightarrow 0$, the optimal protocol follows midpoint interpolation in geodesic space,

$$\mathcal{G}_{\tau \rightarrow 0^+}(A_\alpha) = \frac{1}{2} \left[\mathcal{G}(A_\alpha^i) + \mathcal{G}(A_\alpha^f) \right]. \quad (19)$$

Inverting back to the control parameter space gives $A_\alpha = \mathcal{G}^{-1} \left(\frac{1}{2} \mathcal{G}(A_\alpha^i) + \frac{1}{2} \mathcal{G}(A_\alpha^f) \right)$ in the limit $\tau \rightarrow 0$. $\mathcal{G}_\tau(A_\alpha)$ is plotted in fig. 1(e) for different τ . Due to $\mathcal{G}(A_\alpha) > A_\alpha$, endpoint jumps are amplified for fEQ systems.

Using the finite-time optimal transport map eq. (18), the optimal bulk and boundary EP are

$$\begin{aligned} \Sigma_{\text{bulk}}^* &= \frac{\tau}{2(2 + \tau)^2} \left(\mathcal{G}(A_\alpha^f) - \mathcal{G}(A_\alpha^i) \right)^2, \\ \Sigma_{\text{bnd}}^* &= \frac{2}{2(2 + \tau)^2} \left(\mathcal{G}(A_\alpha^f) - \mathcal{G}(A_\alpha^i) \right)^2. \end{aligned} \quad (20)$$

Equation (20) reveals the fundamental trade-off between bulk and boundary EP in optimal finite-time processes. In particular, $\Sigma_{\text{bulk}}^* \propto \tau$ and $\Sigma_{\text{bnd}}^* \propto 1$, implying that finite-time optimal protocols with *kinks* are a physical manifestation of the optimization interplay between them. The large- τ and small- τ regimes correspond to the domination of Σ_{bulk}^* and Σ_{bnd}^* , respectively, for the thermodynamic optimization. The total optimal driving EP $\Sigma_\tau^* = \Sigma_{\text{bulk}}^* + \Sigma_{\text{bnd}}^*$ is,

$$\Sigma_\tau^* = \frac{1}{2(2 + \tau)} \left(\mathcal{G}(A_\alpha^f) - \mathcal{G}(A_\alpha^i) \right)^2. \quad (21)$$

Compared to eq. (8), Σ_τ^* is finite in the $\tau \rightarrow 0$ limit and smaller than Σ_{qs}^* . They satisfy the non-equilibrium scaling relations $\Sigma_\tau^* \propto 1/(2 + \tau)$ and $\Sigma_{qs}^* \propto 1/\tau$, respectively. Importantly, eq. (21) imposes an upper bound on the driving dissipation $\Sigma_\tau^* \leq \left(\mathcal{G}(A_\alpha^f) - \mathcal{G}(A_\alpha^i) \right)^2 / 4$, saturated in the $\tau \rightarrow 0$ limit. An analogy of an upper bound for the driving dissipation is missing for the slow-driving processes.

Thermodynamically, finite-time optimal driving is equivalent to slow driving with driving time $\tau + 2$ instead of τ . This interpretation is consistent with the dynamic mapping between slow-driving and finite-time optimal protocols elucidated using eqs. (7) and (18). The short-time underestimation from $\Sigma_\tau \propto 1/\tau$ scaling has been experimentally observed [30]. In conclusion, we analytically solve the GFTOC problem by revealing its exact connection to its slow-driving counterpart.

3.2. The physical interpretation of *kinks* and the role of boundary conditions

We elaborate on the physical interpretation of *kinks* within our GFTOC framework. In the small driving-time limit, the fundamental principle of (ST)—the timescale separation between the environment and system degrees of freedom—is violated. This principle normally ensures that the system instantaneously relaxes to the control parameters imposed by

the environment. Simultaneously, the boundary conditions enforce a constraint of reaching the final control parameters within the given finite time τ from the specified initial control parameters. Hence, for small τ , due to violation of the speed-limit bound eq. (13), the environment cannot instantaneously impose the required control parameters on the system.

Kinks solve this issue, as they reduce the geodesic distance for the finite-time driving process, mathematically expressed as $|\mathcal{G}(A_\alpha^{i*}) - \mathcal{G}(A_\alpha^{f*})| < |\mathcal{G}(A_\alpha^i) - \mathcal{G}(A_\alpha^f)|$. This trade-off between the rush to reach the final point along the geodesic and the inability to do so within time τ produces *kinks*. The thermodynamic cost of each *kink* is $\Sigma_{\text{bnd}}^*/2$. The system undergoes a ‘thermodynamic shock’ at the initial and final points, generating a spontaneous discontinuous change in the control parameters, which induces a global transition of the system’s state. Within our framework, Σ_{bnd}^* and Σ_{bulk}^* can be interpreted analogously to heat and work, respectively: heat corresponds to the instantaneous discrete cost of a jump, and work to the continuous driving of control parameters. To our knowledge, this provides a novel thermodynamic understanding of the heat–work dual manifestation of the driving EP in finite-time optimal driven far-from equilibrium processes, which is .

3.3. Finite-time speed limit

Using Σ_{bulk}^* from eq. (20) and eqs. (13) and (16), one finds

$$\tau_\tau^* = \frac{\left(\mathcal{G}(A_\alpha^{f*}) - \mathcal{G}(A_\alpha^{i*}) \right)^2}{2\Sigma_{\text{bulk}}^*} = \tau. \quad (22)$$

This shows that the selection of endpoint jump values $\mathcal{G}(A_\alpha^{i*})$ and $\mathcal{G}(A_\alpha^{f*})$ is constrained to restore the speed-limit bound eq. (13) for the finite-time optimal driving process. Physically, this implies that the allowed endpoint jumps are minimal, just sufficient to restore the finite-time speed-limit constraint for any given τ . This highlights a fundamental symmetry: *kinks* are a non-equilibrium mechanism that circumvents the dynamic constraint of limited driving time quantified by the speed-limit, representing the dynamic counterpart of a ‘thermodynamic shock’.

The upper bound on the total amplitude of *kinks*, $|\Delta_{0^+} \mathcal{G}_\tau(A_\alpha)| + |\Delta_{\tau^-} \mathcal{G}_\tau(A_\alpha)|$, a boundary property, can be obtained using the thermodynamic cost of driving and the distance covered in control parameter space (a bulk property). The equal thermodynamic cost Σ_{bnd}^* for each *kink* results from minimizing Σ_{bnd}^* for a constrained total amplitude of *kinks*. Hence, *kinks* arise from finite driving-time constraints that may prevent reaching the final state along the geodesic. The finite-time optimal protocol restores eq. (13) while minimizing the thermodynamic cost of both *kinks*. Importantly, the slow-driving assumption is broken for any finite τ and does not require $\tau < \tau_{qs}^*$. A continuous change of τ therefore induces a smooth transition from eqs. (7) and (8) to eqs. (17) and (21), with τ as the relevant control parameter. Figure 2

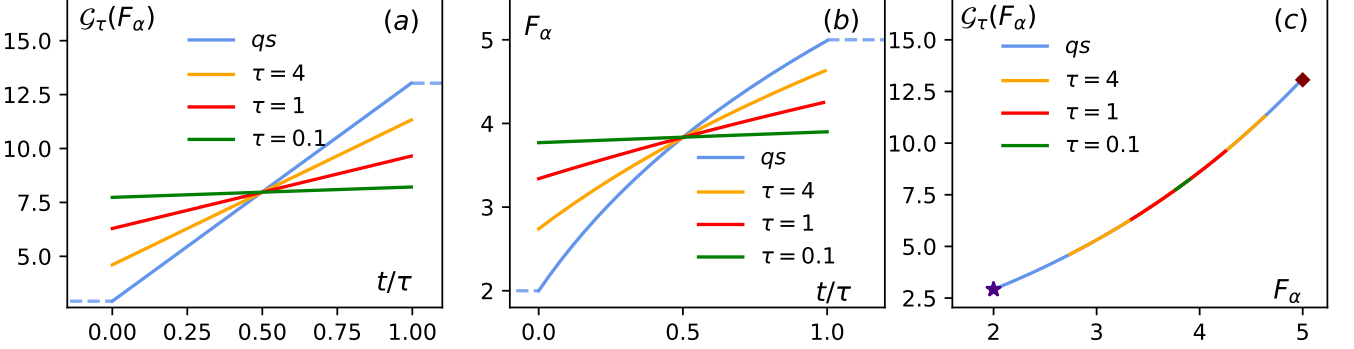


FIG. 2. (a) The finite-time optimal protocol $\mathcal{G}_\tau(F_\alpha) \rightarrow t$ is plotted for the different values of $\tau = \{4, 1, 0.1\}$ with the same initial and final value condition (shown by the dotted blue lines) with $F_\alpha^i = 2$ and $F_\alpha^f = 5$. Its slow-driving counterpart is denoted by ‘qs’. The vanishing excess affinity is considered because the optimal control of the housekeeping EPR is being solved. Where, eqs. (7), (9) and (18) are used for the plot and the scaled (with τ) driving time (t/τ) is used. *Kinks* are of equal amplitude in the geodesic space. (b) The corresponding finite-time non-conservative affinity is obtained using the fEQ geodesic $\mathcal{G}^{fEQ}(F_\alpha)$ in eq. (9), which gives the mapping $F_\alpha \rightarrow t$ in scaled (with τ) driving time (t/τ). *Kinks* are of unequal amplitude in the affinity space, such that a higher mass point exhibits a smaller amplitude of *kinks*. (c) The corresponding mapping in $\mathcal{G}_\tau(F_\alpha) \rightarrow F_\alpha$ space, the initial and final points are denoted by \star and \blacklozenge , respectively. Due to the finite driving time constraint, the finite-time optimal protocol eq. (18) traverses a part of the slow-driving geodesic eq. (7), such that the finite-time speed limit eq. (22) is restored, analogous to the slow-driving speed limit eq. (13). The choice of discontinuous jumps in the finite-time driving protocol is also constrained by equally distributing the thermodynamic cost (Σ_{bnd}^* in eq. (20)) between the initial and final endpoints, which generates a ‘Thermodynamic shock’ at the initial and final time.

pictorially summarizes the underlying geometric structure of GFTOC.

3.4. Time-reversal symmetry of geodesics

Equations (7) and (18) satisfy time-reversal symmetry, as they are invariant under the transformation $\mathcal{G}(A_\alpha^i) \rightarrow \mathcal{G}(A_\alpha^f)$, $\mathcal{G}(A_\alpha^f) \rightarrow \mathcal{G}(A_\alpha^i)$, and $t \rightarrow \tau - t$. This symmetry arises fundamentally from the geodesic structure of the slow-driving process. The symmetric amplitude of *kinks* extends this symmetry to the finite-time geodesic eq. (17).

3.5. The experimental inference of the geodesic and the non-equilibrium scaling relation

GFTOC framework implies that the minimum driving EP is obtained by computing the geodesic. If experimental set-ups can measure the optimal driving EP (thermodynamically constrained to support a minimum dissipation for the driving process), one can pose the inverse problem of reconstructing the geodesic for given initial and final control parameters. The non-equilibrium scaling relation eq. (21) can be used to infer the analytical shape of $\mathcal{G}(A_\alpha)$. For observed (Σ_τ^*, τ) data at fixed A_α^i and A_α^f , the collapse of data yields $\mathcal{G}(A_\alpha^f) - \mathcal{G}(A_\alpha^i) = \sqrt{2(2 + \tau)}\Sigma_\tau^*$. Repeating this procedure for different A_α^i and A_α^f reconstructs $\mathcal{G}(A_\alpha)$ experimentally or numerically. The geodesic shape informs about the non-equilibrium character of the process and the contribution of EP, since it has different analytical dependence on the cEQ and fEQ regimes, as discussed before in section 2.2 and later in section 5.

3.6. Comparison and differences to model-specific known results

Finite-time optimal protocols with *kinks* were analytically computed for a particle in a harmonic trap [7] and recently unified using OMTT [8]. These model-specific results differ from the generalized finite-time framework in three aspects: (i) they optimize the free energy ψ_E using control parameter E , (ii) the boundary conditions used to obtain *kinks* differ, and (iii) the thermodynamic cost of *kinks* is undefined in Ref.[7, 8], leading to the physical interpretation of *kinks* as a boundary artefact.

We shortly summarize the procedure outlined in Ref.[8]. The boundary conditions used in [7, 8] are equivalent to fixing $A_\alpha^{i*} = A_i$ and computing $A_\alpha^{*int} \in (A_\alpha^i, A_\alpha^f)$ that minimises the bulk driving EP under the final value constraint. Thus, $A_\alpha^i \rightarrow A_\alpha^{*int}$ is termed as the feasible driving protocol for the given finite-time τ . Then, A_α^{*int} is used to compute A_α^{*i} and A_α^{*f} by introducing counter-adiabatic driving terms that shifts the initially computed driving protocol $A_\alpha^i \rightarrow A_\alpha^{*int}$ to $A_\alpha^{i*} \rightarrow A_\alpha^{f*}$ in driving time τ , and it generates *kinks* of amplitude $A_\alpha^i - A_\alpha^{*i}$ and $A_\alpha^f - A_\alpha^{*f}$ in the optimal protocol. This implies that the computation of the initial geodesic for the finite-time process is based on the assumption of the absence of *kinks* at the initial time $t = 0$. However, the finite-time optimal protocol $A_\alpha^{i*} \rightarrow A_\alpha^{f*}$ is obtained by shifting this protocol (counter-adiabatic driving) to obtain the *kink* at both $t = 0^+$ and $t = \tau^-$.

This contradicts its formulation of constrained and unconstrained optimization for the initial ($t = 0^+$) and final ($t = \tau^-$) points, respectively. Hence, mathematically, this is interpreted as a boundary term artefact because of the inability of

assigning a thermodynamic cost to kinks within their framework. In contrast, within the minimum action formalism, a thermodynamic cost is inherently assigned for *kinks*, and hence unconstrained optimization is implemented for both initial ($t = 0^+$) and final ($t = \tau^-$) points, signified by a double optimization problem in eq. (14). This implies our optimization framework uses minimum assumptions, equivalently assuming the least information about optimal protocols. This allows us to implement an unconstrained optimization problem in eq. (14) that searches/accesses a wider control parameter space for the optimal protocol.

These differences lead to rather drastic physical results. For example, the short-time optimal protocol eq. (19) is midpoint interpolation in the geodesic space $\mathcal{G}(A_\alpha)$ and not necessarily in control parameter space A_α unless $\mathcal{G}(A_\alpha) = A_\alpha$. Hence, even for short driving time τ , the finite-time optimal protocol eq. (19) respects the Riemannian geometric structure in control parameter space. In contrast, the short-time protocols obtained in Ref. [7, 8] follow a midpoint interpolation in control parameter space. This difference is irrelevant in the case of the optimal control of the trap centre, since $\mathcal{G}(A_\alpha) = A_\alpha$ for the control of the trap centre and the short-time optimal protocols obtained in Ref. [70, 71]. However, $\mathcal{G}(A_\alpha) \neq A_\alpha$ for the optimal control of the trap stiffness [17], giving divergent analytical results compared to Ref. [7, 8, 70, 71]. Subsequently, we will revisit this issue in section 5.5.3 with the example of a stochastic particle in a harmonic trap and reconcile the discrepancies between OMTT [39, 40, 51] and thermodynamic geometry [17].

4. GENERALIZATIONS

4.1. Multiple control parameters

The driving EPR in eq. (5) assumes that all driven control parameters are decoupled and independently driven. However, in practice, there could be cross-couplings between different control parameters. In addition, the transition affinity only accounts for the anti-symmetric part in the transition space [5], and the transition mobility D_α were fixed.

For a slow driving of multiple parameters, the driving Lagrangian is given by:

$$\mathcal{L}_{drv}^* [\lambda] = \frac{1}{2} g_{ij} \dot{\lambda}^i \dot{\lambda}^j, \quad (23)$$

where eq. (23) is represented in Einstein's summation convention, which signifies the summation over the contracted index. $\vec{\lambda}$ is the vector of control parameters. The Hessian of \mathcal{L}^* (mass) gives the metric tensor g_{ij} ,

$$g_{ij} = \begin{bmatrix} \frac{\partial^2}{\partial \lambda^i \partial \lambda^j} \mathcal{L}^* & \frac{\partial \lambda^j}{\partial \lambda^i} \frac{\partial \lambda^i}{\partial \lambda^j} \mathcal{L}^* \\ \frac{\partial \lambda^i}{\partial \lambda^j} \frac{\partial \lambda^j}{\partial \lambda^i} \mathcal{L}^* & \frac{\partial^2}{\partial \lambda^j \partial \lambda^j} \mathcal{L}^* \end{bmatrix}. \quad (24)$$

The MinAP implies solving a variational optimization problem, $\Sigma_{qs}^* = \inf(\Sigma_{drv}^*) = \int_0^\tau dt \mathcal{L}_{drv}^*$. The geodesic equation for the control parameter that minimizes Σ_{drv}^* eq. (23) reads,

$$\ddot{\lambda}_i + \Gamma_{jk}^i \dot{\lambda}_j \dot{\lambda}_k = 0, \quad (25)$$

where the Christoffel symbols are defined as

$$\Gamma_{jk}^i = \frac{1}{2} g^{im} \left(\frac{\partial g_{mj}}{\partial \lambda^k} + \frac{\partial g_{mk}}{\partial \lambda^j} - \frac{\partial g_{jk}}{\partial \lambda^l} \right) \quad (26)$$

Equations (23) and (25) are equivalent to eqs. (5) and (6) for the multi-parameter slow-driving optimal control problem.

By construction, the geodesic $\mathcal{G}(\{\lambda\})$ is the solution that minimizes Σ_{drv}^* , $\mathcal{G}(\{\lambda\}) = \arg \inf_{\{\lambda\}} (\Sigma_{drv}^*)$. The corresponding optimal protocol is the linear interpolation, which reads,

$$\mathcal{G}(\{\lambda\}) = \left(1 - \frac{t}{\tau} \right) \mathcal{G}(\{\lambda^i\}) + \frac{t}{\tau} \mathcal{G}(\{\lambda^f\}). \quad (27)$$

Using eq. (27), the optimal slow driving EP reads:

$$\Sigma_{qs}^* = \frac{1}{2\tau} \left\| \mathcal{G}(\{\lambda^f\}) - \mathcal{G}(\{\lambda^i\}) \right\|^2. \quad (28)$$

The finite-time optimal control framework developed in section 3 is based on the MinAP combined with the existence of the slow-driven geodesic $\mathcal{G}(\{\lambda\})$ and incorporating the possibility of *kinks*. Hence, multi-parameter finite-time optimal control protocol is rather trivial, provided that a slow driving geodesic eq. (27) exists and is computed. The corresponding finite-time multi-parameter optimal protocol reads,

$$\mathcal{G}_\tau(\{\lambda\}) = \left(\frac{1+\tau}{2+\tau} - \frac{t}{2+\tau} \right) \mathcal{G}(\{\lambda^i\}) + \left(\frac{1}{2+\tau} + \frac{t}{2+\tau} \right) \mathcal{G}(\{\lambda^f\}), \quad (29)$$

with the finite-time multi-parameter optimal driving EP reads:

$$\Sigma_\tau^* = \frac{1}{2(2+\tau)} \left\| \mathcal{G}(\{\lambda^f\}) - \mathcal{G}(\{\lambda^i\}) \right\|^2. \quad (30)$$

Equations (27) to (30) are a generalization of eqs. (7), (8), (18) and (21), respectively, for the multi-parameter generalized optimal control problem.

4.2. Numerical computation of geodesic

We have focused on the exact analytical formulation of the GFTOC framework. However, analytically computing the exact geodesic $\mathcal{G}(\{\lambda\})$ is not always feasible for more sophisticated problems. To this end, a numerical framework is required to compute the geodesic/optimal protocols. Here, we highlight two different numerical algorithms that are implemented to calculate the geodesic. The first algorithm is based on the MinAP, where the geodesic $\mathcal{G}(\{\lambda\})$ is obtained by the minimization of the Lagrangian eq. (23), and is extended to return the finite-time optimal protocol $\mathcal{G}_\tau(\{\lambda\})$, it reads,

Algorithm 1 Computing finite-time optimal protocols by minimizing the cost function (action)

Input: A_i, A_f, τ, g_{ij} , eqs. (23), (29) and (30)

- 1: Compute the geodesic $\mathcal{G}(A_\alpha)$ obtained by the recursive minimization of eq. (23), and that connects $\mathcal{G}(A_i)$ and $\mathcal{G}(A_f)$.
- 2: Calculate the finite-time optimal protocol $\mathcal{G}_\tau(t)$ and EP cost Σ_τ^* using eqs. (29) and (30), respectively.
- 3: Return the optimal protocol $\mathcal{G}_\tau(t)$ and EP cost Σ_τ^* .

Note that, *Algorithm 1* is modified to directly compute $\mathcal{G}_\tau(\{\lambda\})$ instead of $\mathcal{G}(\{\lambda\})$, if the thermodynamic cost for *kinks* is assigned under the action minimization problem and the endpoint discontinuity in the protocol space is allowed by relaxing the boundary condition constraint. *Algorithm 1* extends to the class of numerical optimization methods developed in Ref.[24, 52–59] and related to machine learning techniques Ref.[60–62]. However, none of the previous numerical algorithms incorporates *kinks* as a result of their failure to assign a thermodynamic cost to *kinks*. To our knowledge, *Algorithm 1* is the novel formulation that numerically computes finite-time optimal protocols with *kinks* and computes the associated finite-time driving EP cost.

A second alternative algorithm computes the finite-time optimal protocols by numerically solving the geodesic eq. (25) as a boundary value problem. The algorithm for it reads:

Algorithm 2 Computing finite-time optimal protocols by numerically solving geodesic ODEs

Input: $A_i, A_f, \tau, g_{ij}, \Gamma_{ij}^k$, eq. (25) and eq. (29)

- 1: Compute the geodesic $\mathcal{G}(A_\alpha)$ by numerically solving eq. (25) under the boundary value constraint A_i and A_f at $t = 0$ and $t = \tau$.
- 2: Calculate the finite-time optimal protocol $\mathcal{G}_\tau(t)$ and EP cost Σ_τ^* using eqs. (29) and (30), respectively.
- 3: Return the optimal protocol $\mathcal{G}_\tau(t)$ and EP cost Σ_τ^* .

In contrast to *Algorithm 1*, *Algorithm 2* can only compute $\mathcal{G}(A_\alpha)$, and requires eq. (29) to compute $\mathcal{G}_\tau(A_\alpha)$. The numerical approach elaborated in this section broadens the applicability of the GFTOC when an exact analytical solution of the geodesic is not available.

5. APPLICATIONS OF GFTOC FRAMEWORK

5.1. Linear optimal control

Linear irreversible thermodynamics utilizes the most fundamental quadratic dissipation function $\mathcal{L}^* = kA_\alpha^2$ for the EPR [72, 73]. This leads to $\mathcal{L}_{drv}^* = kA_\alpha^2$ with the mass $\partial_{A_\alpha}^2 \mathcal{L}^* = 2k$. Fixing $k = 1/2$ implies a unit mass. Solving $\dot{A}_\alpha = v_{qs}$ gives $\mathcal{G}^{lin}(A_\alpha) = A_\alpha$. Thus, the geodesic is a linear interpolation between A_α^i and A_α^f in A_α space, and the slow driving optimal EP and the corresponding optimal protocol

read,

$$\begin{aligned} \Sigma_{qs}^* &= \frac{1}{2\tau} (A_f - A_i)^2, \\ A_\alpha(t) &= \left(1 - \frac{t}{\tau}\right) A_\alpha^i + \frac{t}{\tau} A_\alpha^f, \end{aligned} \quad (31)$$

respectively. The optimal finite-time driving EP and the corresponding optimal finite-time protocol read,

$$\begin{aligned} \Sigma_\tau^* &= \frac{1}{2(2+\tau)} (A_f - A_i)^2, \\ A_\alpha(t) &= \left(\frac{1+\tau}{2+\tau} - \frac{t}{2+\tau}\right) A_\alpha^i + \left(\frac{1}{2+\tau} + \frac{t}{2+\tau}\right) A_\alpha^f. \end{aligned} \quad (32)$$

The linear optimal control formulated here is a trivial example of Euclidean geometry with a constant mass.

5.2. Optimal control of free energy

The EP defined for the driving of the free energy ψ_E by changing the control parameters $\{\lambda\}$ of E reads, $\mathcal{L}_{drv}^* = \frac{1}{2} (\partial^2 \psi_E / \partial \lambda_i \partial \lambda_j) \dot{\lambda}_i \dot{\lambda}_j$. The initial and final control parameter vectors are denoted by $\vec{\lambda}_E^{inl}$ and $\vec{\lambda}_E^{fnl}$, respectively. The corresponding optimal slow driving EP and the optimal driving protocol read:

$$\begin{aligned} \Sigma_{qs}^* &= \frac{1}{2\tau} \left(\mathcal{G}(\vec{\lambda}_E^{inl}) - \mathcal{G}(\vec{\lambda}_E^{fnl}) \right)^2, \\ \mathcal{G}(\vec{\lambda}) &= \left(1 - \frac{t}{\tau}\right) \mathcal{G}(\vec{\lambda}_E^{inl}) + \frac{t}{\tau} \mathcal{G}(\vec{\lambda}_E^{fnl}). \end{aligned} \quad (33)$$

The corresponding optimal finite-time EP and the optimal finite-time driving protocol read:

$$\begin{aligned} \Sigma_\tau^* &= \frac{1}{2(2+\tau)} \left(\mathcal{G}(\vec{\lambda}_E^{inl}) - \mathcal{G}(\vec{\lambda}_E^{fnl}) \right)^2, \\ \mathcal{G}_\tau(\vec{\lambda}_E) &= \left(\frac{1+\tau}{2+\tau} - \frac{t}{2+\tau}\right) \mathcal{G}(\vec{\lambda}_E^{inl}) + \left(\frac{1}{2+\tau} + \frac{t}{2+\tau}\right) \mathcal{G}(\vec{\lambda}_E^{fnl}). \end{aligned} \quad (34)$$

Note that the exact geodesic functions $\mathcal{G}(\vec{\lambda}_E)$ are model-specific, due to the different analytical dependence of ψ_E on λ_E [19–21]. But in the next section, we explicitly compute the geodesic functions $\mathcal{G}(\vec{\lambda}_E)$ for a stochastic particle in a harmonic trap.

5.3. Stochastic particle in a harmonic trap and Wasserstein distance for the Gaussian distribution

A stochastic particle in a harmonic trap potential models an important equivalence class that describes a large class of physical systems, and hence has been the testbed of novel theoretical developments in ST. The stochastic particle satisfies the Boltzmann distribution, $P \propto e^{-k(x-m)^2}$, with the

trap stiffness k and centre m . In this case, these two relevant control parameters fully capture the statistical properties of the system. We consider a finite-time optimal control problem for the time-dependent change of the trap stiffness $k(t)$ and centre $m(t)$ [7, 17]. The inverse of the trap stiffness quantifies the covariance (C) of the Gaussian distribution for the particle position, $C \propto 1/k$ [7]. Hence, by definition, the finite-time optimal control formulation for changing the centre and stiffness of the harmonic trap is equivalent to the optimal transport theory to change the mean and covariance of the Gaussian distribution for the position of the particles [39]. However, the results obtained from different methods do not match [7, 39, 51]. We resolve these discrepancies using the GFTOC framework.

We consider an optimal control problem for changing the trap stiffness and centre from (m_i, k_i) to (m_f, k_f) . The mass for the centre and the stiffness of the trap are $g_{mm} = 1$ and $g_{kk} = 1/k^3$ [17]. This implies the geodesic function $\mathcal{G}(m) = m$ and $\mathcal{G}(k) = k^{-1/2}$. Using $C \propto 1/k$, we recover the geodesic function $\mathcal{G}(C) = C^{1/2}$ for the covariance. Hence, the minimum slow driving EP and the corresponding optimal protocols for the mean and variance read:

$$\Sigma_{qs}^* = \frac{1}{2\tau} \left[(m_f - m_i)^2 + \left(\sqrt{C_f} - \sqrt{C_i} \right)^2 \right]. \quad (35a)$$

$$m_\tau(t) = \left(1 - \frac{t}{\tau} \right) m_i + \frac{t}{\tau} m_f \quad (35b)$$

$$\sqrt{C_\tau(t)} = \left(1 - \frac{t}{\tau} \right) \sqrt{C_i} + \frac{t}{\tau} \sqrt{C_f} \quad (35c)$$

Equation (35a) is the \mathcal{W}_2 Wasserstein distance between the initial and final Gaussian probability distributions Ref. [39, 40, 44] with the corresponding optimal protocols for the mean and covariance eqs. (35b) and (35c) mentioned in Ref.[39].

Further, applying the GFTOC framework, the minimum finite-time driving EP and finite-time optimal protocols for the mean and variance read:

$$\Sigma_\tau^* = \frac{1}{2(2+\tau)} \left[(m_f - m_i)^2 + \left(\sqrt{C_f} - \sqrt{C_i} \right)^2 \right]. \quad (36a)$$

$$m_\tau(t) = \left(\frac{1+\tau}{2+\tau} - \frac{t}{2+\tau} \right) m_i + \left(\frac{1}{2+\tau} + \frac{t}{2+\tau} \right) m_f \quad (36b)$$

$$\sqrt{C_\tau(t)} = \left(\frac{1+\tau}{2+\tau} - \frac{t}{2+\tau} \right) \sqrt{C_i} + \left(\frac{1}{2+\tau} + \frac{t}{2+\tau} \right) \sqrt{C_f} \quad (36c)$$

Equation (36a) is the novel formulation of the finite-time Wasserstein distance between the initial and final Gaussian probability distributions; it is less than eq. (35a) due to *kinks*. The finite-time optimal protocol for the center of the trap eq. (36b) is the same as Ref.[7, 8]. However, the finite-time optimal protocol for the trap stiffness eq. (36c) is different from Refs. [7, 8]. These differences, due to boundary conditions and their physical implications, have previously been detailed in section 3.3.6.

5.4. Optimal control of excess EP

The optimal control formulation has been developed for the affinity, which lies in the transition space. However, as previously shown in eq. (2), a part of the EPR can be integrated to obtain the excess EP $\Sigma^{ex} = -D_E^{KL}$, which is defined in the state space. The integration is implemented: 1) from the transition space to the state space, and 2) in time. This implies that Σ^{ex} is the boundary term that does not require knowledge of the transition-space topology. This property of the excess EP has been exploited in the literature so far to formulate the control or geodesic description of cEQ systems [16, 44, 74, 75]. For $-\Sigma^{ex} = \sum_{\{i\}} \rho_i \log(\rho_i/\rho_i^E)$, the mass is equal to the stochastic Fisher information $\partial_{\rho_i}^2 \Sigma^{ex} = 1/\rho_i$ defined with respect to ρ_i [76]. Reorganization of $\Sigma_{drv}^{ex} = \sum_{\{i\}} (\partial_t \rho_i)^2 / 2\rho_i$ leads to $\Sigma_{drv}^{ex} = \sum_{\{i\}} \rho_i [\partial_t \log(\rho_i/\rho_i^E)]^2$, the quadratic form of the excess driving EP written in terms of the driving of the excess affinity $A_i^{ex} = -\log(\rho_i/\rho_i^E)$. Thus, the control of the state is equivalent to the control of the excess affinity. It is equal to the Fisher information defined for the state distribution $\{\rho_i\}$. To avoid confusion with the state index, we introduce a short-hand notation $\vec{\rho}(\tau)$ and $\vec{\rho}(0)$ for the final and initial states of the system represented as component-wise vectors.

Using $\mathcal{L}_{drv}^{ex} = \sum_{\{i\}} (\partial_t \rho_i)^2 / 2\rho_i$ leads to $\mathcal{G}(\rho_i) = 2\sqrt{\rho_i}$ and resolves $\Sigma_{drv}^{ex} = \int_0^\tau \mathcal{L}_{drv}^{ex} dt$. The corresponding slow-driving optimal excess EP and the optimal driving protocol read:

$$\Sigma_{qs}^{*ex} = \frac{2}{\tau} \left(\sqrt{\vec{\rho}(\tau)} - \sqrt{\vec{\rho}(0)} \right)^2, \quad (37a)$$

$$\sqrt{\vec{\rho}(t)} = \left(1 - \frac{t}{\tau} \right) \sqrt{\vec{\rho}(0)} + \frac{t}{\tau} \sqrt{\vec{\rho}(\tau)}. \quad (37b)$$

Equation (37a) is the cEQ slow-driving formulation with a quadratic relation between the thermodynamic length and the excess EP [74, 75]. However, the corresponding optimal slow-driving protocol eq. (37b) is novel.

Furthermore, the solution of the GFTOC problem for excess EP leads to the optimal finite-time excess EP and the finite-time optimal driving protocol, which read:

$$\Sigma_\tau^{*ex} = \frac{2}{(2+\tau)} \left(\sqrt{\vec{\rho}(\tau)} - \sqrt{\vec{\rho}(0)} \right)^2, \quad (38a)$$

$$\sqrt{\vec{\rho}_\tau(t)} = \left(\frac{1+\tau}{2+\tau} - \frac{t}{2+\tau} \right) \sqrt{\vec{\rho}(0)} + \left(\frac{1}{2+\tau} + \frac{t}{2+\tau} \right) \sqrt{\vec{\rho}(\tau)}. \quad (38b)$$

Equation (38a) reveals that the ‘thermodynamic shock’ lowers the driving cost of excess EP due to *kinks* in $\sqrt{\vec{\rho}_\tau(t)}$. Within infinitesimal time at the initial and final driving times, the state of the system undergoes an instantaneous simultaneous jump. Importantly, eqs. (37) and (38) are constrained by the conservation law manifold. Therefore, they can be further simplified/sophisticated to obtain eqs. (37) and (38) as a function of the linearly independent state space whose dimension is reduced exactly by the total number of conservation laws.

5.5. Optimal control of housekeeping EPR

Using the housekeeping EPR in eq. (2), we formulate the optimal control problem for $\dot{\Sigma}_{hk}$ using the external control of F_α from an initial to a final value F_α^i to F_α^f . Physically, this implies that the control parameters $\{\lambda_E\}$ of E are fixed and the state-space distribution is in steady state. This leads to vanishing driving work and excess EPR contributions, respectively. The driving Lagrangian for the EPR of housekeeping then reads $\mathcal{L}_{drv}^* = \frac{1}{2} \partial_{F_\alpha}^2 \mathcal{L}_{hk}^* (\dot{F}_\alpha)^2$. The mass for the driving reads, $\partial_{F_\alpha}^2 \mathcal{L}_{hk}^* = T_\alpha^\perp \cosh(F_\alpha/2) + T_\alpha^\perp F_\alpha \sinh(F_\alpha/2)/4$. It is rewritten as $\partial_{F_\alpha}^2 \mathcal{L}_{hk}^* = \frac{1}{2} \left(T_\alpha(A_\alpha) + T_\alpha(A_\alpha^\dagger) \right) + \frac{1}{4} \dot{\Sigma}_{\alpha}^{hk}$ with the total affinity $A_\alpha = F_\alpha + A_\alpha^{ex}$ and $A_\alpha^\dagger = F_\alpha - A_\alpha^{ex}$ being the affinity obtained by the time-reversal of the boundary term. Using the orthogonal symmetry of the non-equilibrium fluctuations, $T_\alpha(A_\alpha) = T_\alpha(A_\alpha^\dagger)$, the mass is reduced to, $\partial_{F_\alpha}^2 \mathcal{L}_{hk}^* = T_\alpha + \dot{\Sigma}_{\alpha}^{hk}/4$. Hence, for driving the fEQ F_α , the mass is proportional to the traffic T_α and the housekeeping EPR $\dot{\Sigma}_{\alpha}^{hk}$ due to the bidirectional transition α , and increases exponentially as the system is further from equilibrium due to the hyperbolic scalings of T_α and $\dot{\Sigma}_{\alpha}$. This reveals that the higher housekeeping EPR and non-equilibrium fluctuations generate higher driving resistance. We use an exponential approximation of the hyperbolic functions, which is valid for fEQ systems, and use a previously computed closed-form analytical expression for the fEQ geodesic \mathcal{G}^{fEQ} in eq. (9).

The solution of the slow-driving optimal control problem for the housekeeping EPR leads to the optimal driving EP and the corresponding optimal protocol,

$$\begin{aligned} \Sigma_{qs}^{*hk} &= \frac{1}{2\tau} \left(\mathcal{G}^{fEQ}(F_\alpha^f) - \mathcal{G}^{fEQ}(F_\alpha^i) \right)^2, \\ \mathcal{G}^{fEQ}(F_\alpha) &= \left(1 - \frac{t}{\tau} \right) \mathcal{G}^{fEQ}(F_\alpha^i) + \frac{t}{\tau} \mathcal{G}^{fEQ}(F_\alpha^f). \end{aligned} \quad (39)$$

Similarly, the solution of the finite-time optimal control problem for the housekeeping EPR leads to the optimal finite-time driving EP and the corresponding finite-time optimal protocol, which are,

$$\begin{aligned} \Sigma_\tau^{*hk} &= \frac{1}{2(2+\tau)} \left(\mathcal{G}^{fEQ}(F_\alpha^f) - \mathcal{G}^{fEQ}(F_\alpha^i) \right)^2, \\ \mathcal{G}^{fEQ}(F_\alpha) &= \left(\frac{1+\tau}{2+\tau} - \frac{t}{2+\tau} \right) \mathcal{G}^{fEQ}(F_\alpha^i) \\ &\quad + \left(\frac{1}{2+\tau} + \frac{t}{2+\tau} \right) \mathcal{G}^{fEQ}(F_\alpha^f). \end{aligned} \quad (40)$$

A pictorial representation of the optimal control of F_α is shown in fig. 2 and pictorially summarizes the essence of this work.

5.6. Multi-parameter optimal control of affinity and mobility

We show the applicability of the multi-parameter optimal control. We incorporate the symmetric part of the transition,

namely mobility D_α , which was previously fixed. This implies $\{\lambda_\alpha^i\} = \{A_\alpha, D_\alpha\}, \forall \alpha \in \{\gamma^\pm\}$. Henceforth, we use the shorthand notation $a = A_\alpha$ and $d = D_\alpha$ for brevity. Using \mathcal{L}^* , the exact metric tensor for the simultaneous control of mobility D_α and affinity A_α reads

$$g_{ij} = \begin{bmatrix} 2d \left[\cosh\left(\frac{a}{2}\right) + \frac{a}{2} \sinh\left(\frac{a}{2}\right) \right] & \left[a \cosh\left(\frac{a}{2}\right) + 2 \sinh\left(\frac{a}{2}\right) \right] \\ \left[a \cosh\left(\frac{a}{2}\right) + 2 \sinh\left(\frac{a}{2}\right) \right] & 0 \end{bmatrix}. \quad (41)$$

Using eqs. (26) and (41), the exact expression for the Christoffel symbols reads,

$$\begin{aligned} \Gamma_{aa}^a &= \left(1 + \frac{a}{4} \tanh\left(\frac{a}{2}\right) \right) / \left(a + 2 \tanh\left(\frac{a}{2}\right) \right), \\ \Gamma_{da}^d &= \Gamma_{ad}^d = \left(1 + \frac{a}{4} \tanh\left(\frac{a}{2}\right) \right) / \left(a + 2 \tanh\left(\frac{a}{2}\right) \right), \\ \Gamma_{aa}^d &= d(-14 + a^2 - 2 \cosh(a)) / \left(8 \left[a \cosh\left(\frac{a}{2}\right) + 2 \sinh\left(\frac{a}{2}\right) \right]^2 \right), \\ \Gamma_{ad}^a &= \Gamma_{da}^a = \Gamma_{dd}^a = \Gamma_{dd}^d = 0. \end{aligned} \quad (42)$$

The exact geodesic eq. (25) for the optimal control of transition affinity and mobility is reduced to,

$$\ddot{A}_\alpha + \Gamma_{aa}^a \dot{A}_\alpha^2 = 0 \quad (43a)$$

$$\ddot{D}_\alpha + \Gamma_{aa}^d \dot{A}_\alpha^2 + 2\Gamma_{ad}^d \dot{A}_\alpha \dot{D}_\alpha = 0 \quad (43b)$$

Equation (43a) for the optimal driving of the affinity is the same as eq. (6), and does not depend on D_α . Therefore, the optimal driving dynamics of the mobility D_α given by eq. (43b) are enslaved by the geodesic for A_α . This implies that an optimal control problem for transition affinity and mobility can be reduced to two steps. First step, to solve the optimal control problem A_α , as formulated in sections 2 and 3, and obtain the geodesic $\mathcal{G}(A_\alpha)$. Second step, plugging $\mathcal{G}(A_\alpha)$ into eq. (43b) and solving ODE eq. (43b) for optimal driving of D_α , and obtain the geodesic $\mathcal{G}(A_\alpha, D_\alpha)$. We cannot find an exact analytical solution for the geodesic $\mathcal{G}(A_\alpha, D_\alpha)$ due to the sophistication associated with solving coupled ODEs. However, the numerical computation of $\mathcal{G}(A_\alpha, D_\alpha)$ is always feasible.

6. CONCLUSION AND OUTLOOK

We consider a finite-time optimal control problem for driving the control parameters of discrete-state systems from the initial to the final value, such that the EPR for driving is minimised. Building upon the ‘minimum action principle’ (MinAP), we propose a framework for the generalized finite-time optimal control (GFTOC). The ‘minimum action principle’ allows for a variational formulation of the finite-time optimal control problem. To solve this problem, we develop a two-step solution. In the first step, assuming slow driving, we solve the slow driving optimal control problem by exploiting the Riemannian geometry induced in the manifold of control parameters. This approach unifies and generalizes the

thermodynamic geometry and the OMTT for fEQ systems. Then, the dissipation-minimizing optimal paths are obtained by the geodesic, the minimum-distance path on the Riemannian manifold.

In the second step, we investigate the possibility of discontinuous endpoint jumps in the optimal protocol by relaxing the assumption of slow driving. We utilize the slow-driving geodesic obtained to compute the finite-time geodesic; our analysis reveals an exact mapping between the slow-driving and finite-time optimal control problem. This strong and important result allows us to extend the framework of thermodynamic geometry developed for slowly driven systems to systems driven in any finite time. Importantly, due to the ‘minimum action principle’, a thermodynamic cost is assigned to the endpoint jumps; this instantaneous dissipation cost at the endpoints is termed a ‘thermodynamic shock’. We analytically prove that it is a model-independent generic mechanism for far-from-equilibrium (fEQ) systems, which reduces the driving dissipation cost. Within our framework, discontinuous endpoint jumps in the optimal protocol are a physical manifestation of a ‘thermodynamic shock’, implying that the optimal driven dynamics are constrained by thermodynamics.

Our framework opens up a plethora of practical applications in biology, chemistry, and nanoscale / mesoscale devices, where stochastic thermodynamics has been an experimentally tested theoretical paradigm [4]. Our framework opens the door for the experimental design, optimization, and control of such systems. The experimental verification of our framework awaits exploration [30]. The GFTOC framework is rather trivially extended to quantum systems, as the development of optimal control and speed limits for quantum systems is attributed to the underlying geometric structure and not to the quantum nature [77–79].

ACKNOWLEDGMENTS

ATM thanks Jin-Fu Chen for pointing out the experimental work Ref.[30], which motivated the theoretical formulation of the GFTOC problem.

References

- [1] N. Shiraishi, *An Introduction to Stochastic Thermodynamics: From Basic to Advanced* (Springer Nature Singapore, Singapore, 2023) pp. 31–47.
- [2] U. Seifert, Stochastic thermodynamics, fluctuation theorems and molecular machines, *Reports on Progress in Physics* **75**, 126001 (2012).
- [3] K. Sekimoto, *Stochastic Energetics* (Courier Corporation, 2010).
- [4] S. Ciliberto, Experiments in stochastic thermodynamics: Short history and perspectives, *Phys. Rev. X* **7**, 021051 (2017).
- [5] A. T. Mohite and H. Rieger, Stochastic thermodynamics of non-reciprocally interacting particles and fields (2025), [arXiv:2504.10515 \[cond-mat.stat-mech\]](https://arxiv.org/abs/2504.10515).
- [6] J. M. Horowitz and T. R. Gingrich, Thermodynamic uncertainty relations constrain non-equilibrium fluctuations, *Nature Physics* **16**, 15 (2020).
- [7] T. Schmiedl and U. Seifert, Optimal finite-time processes in stochastic thermodynamics, *Phys. Rev. Lett.* **98**, 108301 (2007).
- [8] A. Zhong and M. R. DeWeese, Beyond linear response: Equivalence between thermodynamic geometry and optimal transport, *Phys. Rev. Lett.* **133**, 057102 (2024).
- [9] A. Gomez-Marin, T. Schmiedl, and U. Seifert, Optimal protocols for minimal work processes in underdamped stochastic thermodynamics, *The Journal of Chemical Physics* **129**, 024114 (2008).
- [10] H. Then and A. Engel, Computing the optimal protocol for finite-time processes in stochastic thermodynamics, *Phys. Rev. E* **77**, 041105 (2008).
- [11] M. V. S. Bonança and S. Deffner, Minimal dissipation in processes far from equilibrium, *Phys. Rev. E* **98**, 042103 (2018).
- [12] M. C. Engel, J. A. Smith, and M. P. Brenner, Optimal control of nonequilibrium systems through automatic differentiation, *Phys. Rev. X* **13**, 041032 (2023).
- [13] P. Salamon, J. D. Nulton, and R. S. Berry, Length in statistical thermodynamics, *J. Chem. Phys.* **82**, 2433 (1985).
- [14] D. Brody and N. Rivier, Geometrical aspects of statistical mechanics, *Phys. Rev. E* **51**, 1006 (1995).
- [15] F. Schlögl, Thermodynamic metric and stochastic measures, *Zeitschrift für Physik B Condensed Matter* **59**, 449 (1985).
- [16] G. E. Crooks, Measuring thermodynamic length, *Phys. Rev. Lett.* **99**, 100602 (2007).
- [17] D. A. Sivak and G. E. Crooks, Thermodynamic metrics and optimal paths, *Phys. Rev. Lett.* **108**, 190602 (2012).
- [18] D. Mandal and C. Jarzynski, Analysis of slow transitions between nonequilibrium steady states, *Journal of Statistical Mechanics: Theory and Experiment* **2016**, 063204 (2016).
- [19] D. A. Sivak and G. E. Crooks, Thermodynamic geometry of minimum-dissipation driven barrier crossing, *Phys. Rev. E* **94**, 052106 (2016).
- [20] P. R. Zulkowski, D. A. Sivak, G. E. Crooks, and M. R. DeWeese, Geometry of thermodynamic control, *Phys. Rev. E* **86**, 041148 (2012).
- [21] P. R. Zulkowski, D. A. Sivak, and M. R. DeWeese, Optimal control of transitions between nonequilibrium steady states, *PLOS ONE* **8**, 1 (2013).
- [22] P. R. Zulkowski and M. R. DeWeese, Optimal finite-time erasure of a classical bit, *Phys. Rev. E* **89**, 052140 (2014).
- [23] P. R. Zulkowski and M. R. DeWeese, Optimal protocols for slowly driven quantum systems, *Phys. Rev. E* **92**, 032113 (2015).
- [24] G. M. Rotskoff, G. E. Crooks, and E. Vanden-Eijnden, Geometric approach to optimal nonequilibrium control: Minimizing dissipation in nanomagnetic spin systems, *Phys. Rev. E* **95**, 012148 (2017).
- [25] D. Loutchko, Y. Sugiyama, and T. J. Kobayashi, Riemannian geometry of optimal driving and thermodynamic length and its application to chemical reaction networks, *Phys. Rev. Res.* **4**, 043049 (2022).
- [26] J.-F. Chen, C. P. Sun, and H. Dong, Extrapolating the thermodynamic length with finite-time measurements, *Phys. Rev. E*

104, 034117 (2021).

[27] G. Li, J.-F. Chen, C. P. Sun, and H. Dong, Geodesic path for the minimal energy cost in shortcuts to isothermality, *Phys. Rev. Lett.* **128**, 230603 (2022).

[28] G. Watanabe and Y. Minami, Finite-time thermodynamics of fluctuations in microscopic heat engines, *Phys. Rev. Res.* **4**, L012008 (2022).

[29] S. Ito and A. Dechant, Stochastic time evolution, information geometry, and the cramér-rao bound, *Phys. Rev. X* **10**, 021056 (2020).

[30] Y.-H. Ma, R.-X. Zhai, J. Chen, C. P. Sun, and H. Dong, Experimental test of the $1/\tau$ -scaling entropy generation in finite-time thermodynamics, *Phys. Rev. Lett.* **125**, 210601 (2020).

[31] R. Jordan, D. Kinderlehrer, and F. Otto, The variational formulation of the fokker-planck equation, *SIAM Journal on Mathematical Analysis* **29**, 1 (1998).

[32] J.-D. Benamou and Y. Brenier, A computational fluid mechanics solution to the monge-kantorovich mass transfer problem, *Numerische Mathematik* **84**, 375 (2000).

[33] C. Villani, *Topics in Optimal Transportation* (American Mathematical Society) (American Mathematical Society, Providence, 2003).

[34] F. Santambrogio, *Optimal Transport for Applied Mathematicians(Progress in Nonlinear Differential Equations and Their Applications Volume 87)* (Springer, 2015).

[35] E. Aurell, C. Mejía-Monasterio, and P. Muratore-Ginanneschi, Optimal protocols and optimal transport in stochastic thermodynamics, *Physical review letters* **106**, 250601 (2011).

[36] E. Aurell, C. Mejía-Monasterio, and P. Muratore-Ginanneschi, Boundary layers in stochastic thermodynamics, *Phys. Rev. E* **85**, 020103 (2012).

[37] E. Aurell, K. Gawedzki, C. Mejía-Monasterio, R. Mohayaee, and P. Muratore-Ginanneschi, Refined second law of thermodynamics for fast random processes, *Journal of Statistical Physics* **147**, 487 (2012).

[38] Y. Chen, T. T. Georgiou, and A. Tannenbaum, Stochastic control and nonequilibrium thermodynamics: Fundamental limits, *IEEE transactions on automatic control* **65**, 2979 (2019).

[39] A. Dechant and Y. Sakurai, Thermodynamic interpretation of wasserstein distance (2019), [arXiv:1912.08405 \[cond-mat.stat-mech\]](https://arxiv.org/abs/1912.08405).

[40] M. Nakazato and S. Ito, Geometrical aspects of entropy production in stochastic thermodynamics based on wasserstein distance, *Phys. Rev. Res.* **3**, 043093 (2021).

[41] R. Fu, A. Taghvaei, Y. Chen, and T. T. Georgiou, Maximal power output of a stochastic thermodynamic engine, *Automatica* **123**, 109366 (2021).

[42] A. Taghvaei, O. M. Miangolarra, R. Fu, Y. Chen, and T. T. Georgiou, On the relation between information and power in stochastic thermodynamic engines, *IEEE Control Systems Letters* **6**, 434 (2022).

[43] T. Van Vu and K. Saito, Thermodynamic unification of optimal transport: Thermodynamic uncertainty relation, minimum dissipation, and thermodynamic speed limits, *Phys. Rev. X* **13**, 011013 (2023).

[44] S. Ito, Geometric thermodynamics for the fokker-planck equation: stochastic thermodynamic links between information geometry and optimal transport, *Information Geometry* **7**, 441 (2024).

[45] R. Sabbagh, O. Movilla Miangolarra, and T. T. Georgiou, Wasserstein speed limits for langevin systems, *Phys. Rev. Res.* **6**, 033308 (2024).

[46] J. Klinger and G. M. Rotskoff, Universal energy-speed-accuracy trade-offs in driven nonequilibrium systems, *Phys. Rev. E* **111**, 014114 (2025).

[47] S. Kolouri, S. R. Park, M. Thorpe, D. Slepcev, and G. K. Rohde, Optimal mass transport: Signal processing and machine-learning applications, *IEEE Signal Processing Magazine* **34**, 43 (2017).

[48] A. T. Mohite and H. Rieger, Minimum action principle for entropy production rate of far-from-equilibrium systems () .

[49] A. T. Mohite and H. Rieger, Thermodynamic length in stochastic thermodynamics of far-from-equilibrium systems: Unification of fluctuation relations and thermodynamic uncertainty relations () .

[50] A. T. Mohite and H. Rieger, Thermodynamically consistent coarse-graining: from interacting particles to fields via second quantization (2025), [arXiv:2508.11430 \[cond-mat.stat-mech\]](https://arxiv.org/abs/2508.11430).

[51] S. Oikawa, Y. Nakayama, S. Ito, T. Sagawa, and S. Toyabe, Experimentally achieving minimal dissipation via thermodynamically optimal transport (2025), [arXiv:2503.01200 \[cond-mat.stat-mech\]](https://arxiv.org/abs/2503.01200).

[52] W. E, W. Ren, and E. Vanden-Eijnden, Minimum action method for the study of rare events, *Communications on Pure and Applied Mathematics* **57**, 637 (2004).

[53] M. Heymann and E. Vanden-Eijnden, Pathways of maximum likelihood for rare events in nonequilibrium systems: Application to nucleation in the presence of shear, *Phys. Rev. Lett.* **100**, 140601 (2008).

[54] E. Vanden-Eijnden and M. Heymann, The geometric minimum action method for computing minimum energy paths, *The Journal of Chemical Physics* **128**, 061103 (2008).

[55] T. Grafke, T. Schäfer, and E. Vanden-Eijnden, Long term effects of small random perturbations on dynamical systems: Theoretical and computational tools, in *Recent Progress and Modern Challenges in Applied Mathematics, Modeling and Computational Science*, edited by R. Melnik, R. Makarov, and J. Belair (Springer New York, New York, NY, 2017) pp. 17–55.

[56] T. Grafke and E. Vanden-Eijnden, Numerical computation of rare events via large deviation theory, *Chaos: An Interdisciplinary Journal of Nonlinear Science* **29**, 063118 (2019).

[57] P. Gagran and E. Smith, Action functional gradient descent algorithm for estimating escape paths in stochastic chemical reaction networks, *Phys. Rev. E* **107**, 034305 (2023).

[58] R. Zakine and E. Vanden-Eijnden, Minimum-action method for nonequilibrium phase transitions, *Phys. Rev. X* **13**, 041044 (2023).

[59] E. Smith, H. B. Smith, and J. L. Andersen, Rules, hypergraphs, and probabilities: The three-level analysis of chemical reaction systems and other stochastic stoichiometric population processes, *PLOS Complex Systems* **1**, 1 (2024).

[60] A. Cherukuri, B. Gharesifard, and J. Cortés, Saddle-point dynamics: Conditions for asymptotic stability of saddle points, *SIAM Journal on Control and Optimization* **55**, 486 (2017).

[61] T. Lin, C. Jin, and M. Jordan, On gradient descent ascent for nonconvex-concave minimax problems, in *Proceedings of the 37th International Conference on Machine Learning*, Proceedings of Machine Learning Research, Vol. 119, edited by H. D. III and A. Singh (PMLR, 2020) pp. 6083–6093.

[62] J. Yan, H. Touchette, and G. M. Rotskoff, Learning nonequilibrium control forces to characterize dynamical phase transitions, *Phys. Rev. E* **105**, 024115 (2022).

[63] D.-K. Kim, Y. Bae, S. Lee, and H. Jeong, Learning entropy production via neural networks, *Phys. Rev. Lett.* **125**, 140604 (2020).

[64] S. Otsubo, S. Ito, A. Dechant, and T. Sagawa, Estimating entropy production by machine learning of short-time fluctuating currents, *Phys. Rev. E* **101**, 062106 (2020).

[65] S. K. Manikandan, D. Gupta, and S. Krishnamurthy, Inferring entropy production from short experiments, *Phys. Rev. Lett.* **124**, 120603 (2020).

[66] S. Otsubo, S. K. Manikandan, T. Sagawa, and S. Krishnamurthy, Estimating time-dependent entropy production from non-equilibrium trajectories, *Communications Physics* **5**, 11 (2022).

[67] S. A. Horiguchi and T. J. Kobayashi, Optimal control of stochastic reaction networks with entropic control cost and emergence of mode-switching strategies, *PRX Life* **3**, 033027 (2025).

[68] T. Tottori and T. J. Kobayashi, Theory for optimal estimation and control under resource limitations and its applications to biological information processing and decision-making, *Phys. Rev. Res.* , (2025).

[69] J. Schnakenberg, Network theory of microscopic and macroscopic behavior of master equation systems, *Rev. Mod. Phys.* **48**, 571 (1976).

[70] S. Blaber, M. D. Louwerse, and D. A. Sivak, Steps minimize dissipation in rapidly driven stochastic systems, *Phys. Rev. E* **104**, L022101 (2021).

[71] S. Blaber and D. A. Sivak, Optimal control in stochastic thermodynamics, *Journal of Physics Communications* **7**, 033001 (2023).

[72] L. Onsager and S. Machlup, Fluctuations and irreversible processes, *Phys. Rev.* **91**, 1505 (1953).

[73] S. Machlup and L. Onsager, Fluctuations and irreversible process. ii. systems with kinetic energy, *Phys. Rev.* **91**, 1512 (1953).

[74] H. Qian, Entropy production and excess entropy in a nonequilibrium steady-state of single macromolecules, *Phys. Rev. E* **65**, 021111 (2002).

[75] S. Ito, Stochastic thermodynamic interpretation of information geometry, *Phys. Rev. Lett.* **121**, 030605 (2018).

[76] Note that we use the negative of the excess EP to ensure the positivity of the mass.

[77] M. Okuyama and M. Ohzeki, Quantum speed limit is not quantum, *Phys. Rev. Lett.* **120**, 070402 (2018).

[78] B. Shanahan, A. Chenu, N. Margolus, and A. del Campo, Quantum speed limits across the quantum-to-classical transition, *Phys. Rev. Lett.* **120**, 070401 (2018).

[79] S. B. Nicholson, L. P. García-Pintos, A. del Campo, and J. R. Green, Time-information uncertainty relations in thermodynamics, *Nature Physics* **16**, 1211 (2020).